# Long-Range Exciton Transport by Dynamic Strain Fields in a GaAs Quantum Well

J. Rudolph,* R. Hey, and P. V. Santos

*Paul-Drude-Institut für Festkörperelektronik, Hausvogteiplatz 5-7, D-10117 Berlin, Germany*

(Received 8 January 2007; published 25 July 2007)

We present a novel approach for the microscopic confinement and transport of excitons in GaAs quantum wells (QWs) using the moving strain field of a surface acoustic wave (SAW). We demonstrate that the band-gap modulation induced by the SAW strain field traps long-living indirect excitons in a double QW structure within sub-$\mu$m-wide stripes parallel to the acoustic wave fronts and transports them over several hundreds of $\mu$m.

DOI: 10.1103/PhysRevLett.99.047602 PACS numbers: 77.65.Dq, 71.35.−y, 73.21.−b, 78.55.Cr

Coulomb-coupled electron-hole pairs in semiconductors, so called excitons, play a fundamental role in the interaction with light. Consisting of two fermionic particles, excitons are bosons in the dilute limit and thus susceptible to collective bosonic effects like superfluidity and Bose-Einstein condensation [1–3]. Because of the small exciton effective mass, such effects should be observable at temperatures substantially larger (on the order of 1 K [4]) than for atomic condensates. A major challenge in the search for collective states lies in the control of the excitonic density, motion, and dynamics without dissociating the coupled electron-hole pairs. Several approaches have been proposed to manipulate these neutral particles, including trapping in laser-induced [5] or electrostatic potentials [6], as well as transport by bare diffusion [7], and by drift in potential gradients created by magnetic [8], electric [9,10], or strain [11,12] fields.

In this Letter, we present a novel approach for the simultaneous confinement and transport of excitons in quantum well (QW) structures using the moving strain field of a surface acoustic wave (SAW). We provide experimental evidence for the strain-driven transport of excitons over several hundreds of $\mu$m by using spatially resolved photoluminescence (PL). Furthermore, in contrast to previous approaches, we show that the excitons remain confined within a small spatial range ($\lesssim 1$ $\mu$m), which moves with the well-defined acoustic velocity $v_{\mathrm{SAW}}$. Finally, the low transport velocity $v_{\mathrm{SAW}}$ and the absence of electric fields along the propagation direction prevent exciton heating, thus making the SAW approach a convenient process for the manipulation of cold exciton gases.

Exciton control by SAWs uses the SAW strain field to create—via the deformation potential interaction—a lateral modulation of the conduction (CB) and valence band (VB) edges with amplitudes $\delta E_{\mathrm{CB}}$ and $\delta E_{\mathrm{VB}}$, respectively. The resulting band-gap modulation $\delta E_g = \delta E_{\mathrm{CB}} - \delta E_{\mathrm{VB}}$ is displayed in Fig. 1(a) as a function of the SAW phase $\varphi_{\mathrm{SAW}} = k_{\mathrm{SAW}}x - \omega_{\mathrm{SAW}}t$, where $x$ is the propagation direction while $k_{\mathrm{SAW}} = 2\pi/\lambda_{\mathrm{SAW}}$, $\lambda_{\mathrm{SAW}}$, $\omega_{\mathrm{SAW}}$ denote the acoustic wave vector, wavelength, and angular frequency, respectively. The dynamic band-gap modulation $\delta E_g$ traps and transports excitons stored close to its minima, provided that the exciton mobility $\mu_{\mathrm{ex}}$ is sufficiently large for the drift velocity to exceed $v_{\mathrm{SAW}}$. The experiments were carried out using long-living indirect (or dipolar) excitons in a (Al,Ga)As double QW (DQW) structure on GaAs(001), where the constituent electrons and holes are kept in different QWs separated by a thin (i.e., smaller than the exciton radius) barrier [cf. Figs. 1(b) and 1(c)]. $\delta E_g$ was created by a Rayleigh SAW propagating along the $x = [100]$ surface direction, which does not carry a piezoelectric field. The strain-induced type-I modulation (i.e., with the CB minima and the VB maxima at the same $\varphi_{\mathrm{SAW}}$) and the small electron-hole separation makes the present approach qualitatively different from charge transport by piezoelectric SAWs where the type-II band-gap piezoelectric modulation dissociates excitons and captures the resulting (uncorrelated) electrons and holes at different SAW phases [13,14].

A nonpiezoelectric SAW, however, is not a sufficient condition to ensure a lateral type-I band-gap modulation. To address this point, we display in Fig. 1(d) calculated depth profiles for $E_{\mathrm{CB}}$, $\delta E_{\mathrm{VB}}$, and $\delta E_g$ produced by a SAW with $\lambda_{\mathrm{SAW}} = 5.6$ $\mu$m and a linear power density $P_\ell = 200$ W/m ($P_\ell$ is the acoustic power per unit length perpendicular to the SAW beam). The deformation potential calculations take into account the depth distribution of the acoustic field following the procedure described in Refs. [15,16]. The results are shown for a SAW phase $\varphi_{\mathrm{SAW}}$, where $\delta E_g$ reaches its minimum at the surface (corresponding to $x = 0$ and $z = 0$, respectively). Note that the CB and VB modulations have opposite phases only over a small range of depths (between 0.14 and 0.41 $z/\lambda_{\mathrm{SAW}}$). Based on these results, we chose a depth of 0.27 $\lambda_{\mathrm{SAW}}$ for the DQW, in order to have $\delta E_{\mathrm{CB}} \approx -\delta E_{\mathrm{VB}}$. The corresponding lateral band-gap modulation is displayed in Fig. 1(e).

The structure sketched in Fig. 1(b) was grown by molecular beam epitaxy on an $n^+$-doped GaAs(001) substrate. The undoped DQW, consisting of two 16 nm-wide GaAs QWs coupled by a 4 nm-thick $Al_{0.3}Ga_{0.7}As$ tunnel barrier and cladded by 20 nm $Al_{0.3}Ga_{0.7}As$ outer barriers, was

 

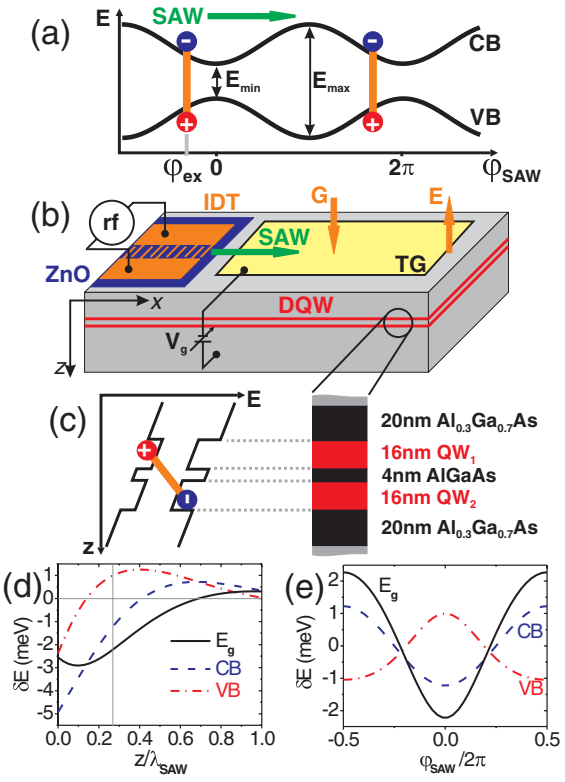


FIG. 1 (color online). (a) Exciton transport by a surface acoustic wave (SAW): The strain field of a SAW along $x = [100]$ creates a moving lateral type-I modulation of the CB and VB's in a DQW [consisting of $QW_1$ and $QW_2$; see (c)], which captures and transports long-living indirect excitons. (b) Sample layout: the SAW is launched by an IDT on a piezoelectric ZnO island. A gate-voltage $V_g$ applied between a semitransparent TG and the doped substrate creates the electric field along $z = [001]$ required for the formation of indirect excitons [see (c)]. The excitons are photogenerated at spot $G$ and transported by the SAW towards the edge $E$ of TG. Calculated (d) depth and (e) lateral (for $z/\lambda_{SAW} = 0.27$) amplitude modulations of the band edges ($\delta E_{CB}$ and $\delta E_{VB}$) and band-gap ($\delta E_g$) induced by a SAW with wavelength $\lambda_{SAW} = 5.6$ $\mu$m and a linear SAW power density $P_\ell = 200$ W/m.

deposited on a 2.5 $\mu$m-thick intrinsic GaAs buffer. The DQW was capped by a 1.5 $\mu$m-thick $Al_{0.1}Ga_{0.9}As$ spacer and a 3 nm GaAs top layer. SAWs travelling along [100] were generated by aluminum interdigital transducers (IDTs) for $\lambda_{SAW} = 5.6$ $\mu$m deposited on a thin (500 nm-thick) piezoelectric ZnO island. The exciton lifetime is controlled by an adjustable electric field along the growth direction, applied via a gate voltage $V_g$ between a semitransparent metallic top-gate (TG) on the SAW propagation path and the doped substrate. Further details about the sample preparation are given in Ref. [17].

Transport measurements were performed on samples mounted in a continuous flow He-cryostat operating at 12 K. Excitons were photogenerated by a 675 nm laser beam focused on a spot $G$ on the top gate [cf. Fig. 1(b)]. The exciton population along the SAW propagation path was tracked by imaging the PL emitted along the SAW path onto the entrance slit of a monochromator, where the PL was spectrally resolved and subsequently recorded with spatial resolution by a CCD camera.

The strain-induced band-gap modulation $\delta E_g$ was directly measured by recording PL spectra from direct excitons (i.e., for $V_g = 0$ V) for different acoustic powers (cf. Fig. 2). For small rf powers $P_{rf} < 6$ dBm, the spectra are dominated by the electron-heavy hole ($e$-$hh$) transition of direct excitons. With increasing SAW power, the $e$-$hh$ line first broadens and then splits into two lines with energies $E_{min}$ and $E_{max}$ [cf. Fig. 1(a)]. The observation of two lines, rather than of a mere PL broadening, results from the large joint density of states at the maximum and minimum of the sinusoidal band-gap modulation [cf. Fig. 1(e)] [15]. The splitting $\Delta E_g = E_{max} - E_{min}$ thus directly yields twice the amplitude $2\delta E_g$ of the band-gap modulation. The measurements are correlated with calculations in the inset of Fig. 2, where the splittings $\Delta E_g$ are plotted as a function of $P_\ell^{1/2}$ (which is proportional to the SAW strain field). Absolute values for $P_\ell$ were determined from the nominal rf-power $P_{rf}$ applied to the IDTs after correction for the coupling losses obtained from rf-reflection measurements. The deformation potential calculations reproduce the measured strain-induced splittings very well. Since the total thickness of the DQW structure is much smaller than $\lambda_{SAW}$, these modulation results also apply for indirect excitons.

The short radiative lifetimes of direct excitons prevent long-range transport by the SAW fields. In fact, the PL intensity in Fig. 2 shifts towards $E_{min}$ for high SAW powers, thus indicating that these excitons are locally transported (i.e., within a SAW cycle) towards the minima of the type-I modulation. The total integrated PL intensity, however, remains approximately constant with $P_{rf}$, thus confirming that no long-range transport takes place. The

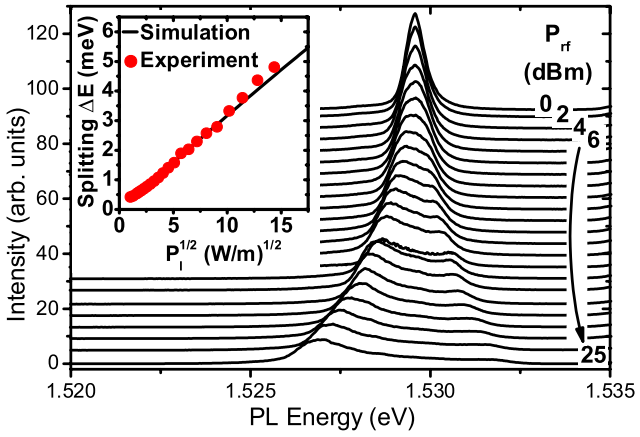


FIG. 2 (color online). PL spectra from direct excitons for different rf powers $P_{rf}$ applied to the IDT. The inset compares the PL splitting ($\Delta E_g$, dots) with the calculated band-gap modulation ($=2\delta E_g$, line).

situation changes if a negative gate voltage $V_g$ is applied to create long-living indirect excitons below the top gate TG [cf. Fig. 1(b)]. We consider first the long-range diffusion indicated by the dashed lines in Fig. 3, which compare spatially resolved profiles for the PL from indirect excitons recorded for different voltages in the absence of a SAW. Here, the PL intensity was integrated both spectrally over the *e-hh* emission line and spatially across the SAW beam width. The increased exciton lifetime $\tau_{ex}$ for large negative bias ($V_g < -6$ V) leads to an exponential diffusion tail away from the generation point $x = 0$ with a decay length $L_{ex} = \sqrt{D_{ex}\tau_{ex}}$, where $L_{ex}$ and $D_{ex}$ are the exciton diffusion length and diffusion coefficient, respectively. Simultaneously, the PL intensity from the generation spot ($x = 0$ $\mu$m) reduces due to the decreasing overlap of the electron and hole wave functions. The $L_{ex}$ obtained from the profiles for negative $x$ (where the top-gate extends to $x = -1200$ $\mu$m) are displayed in the inset of the figure.

The remarkable increase in lifetime induced by large negative gate voltages ($V_g < -6$ V in Fig. 3) leads to essentially flat PL tails for $x > 0$, as $L_{ex}$ becomes comparable to the distance between the generation point and the edge of the top gate (which extends to $x \approx 265$ $\mu$m in Fig. 3). Under these conditions, the exciton lifetime is limited by the screening of the applied electric field due to a large density of dipolar excitons in the DQW structure. This self-limiting lifetime determines the ultimate exciton population under the top gate induced by continuous illumination.

Direct evidence for SAW-induced long-range exciton transport is provided by the solid curves in Fig. 3, which were recorded under the same conditions as the dashed ones except for the application of a nominal power $P_{rf} =$ 24 dBm to the IDT. No SAW effects are observed in the region of short exciton lifetimes (i.e., for $0 > V_g \geq -4$ V). For $V_g < -4$ V, the PL tail along the transport direction becomes more pronounced, thus demonstrating the onset of long-range acoustic transport. Simultaneously, exciton diffusion against the SAW propagation direction is suppressed, as indicated by the reduced PL for negative $x$. The transport efficiency increases dramatically for more negative voltages ($V_g \leq -6$ V), leading to a strong emission from the edge $E$ of the top-gate ($x = 265$ $\mu$m). Transport beyond $E$ is hindered by the potential barrier induced by the quantum-confined Stark effect (QCSE) that creates a potential well for indirect excitons below the top gate [6]. As excitons approach the edge of the top-gate, their lifetime decreases following the reduction of the vertical component of the applied electric field.

The dependence of the transport efficiency on SAW power is displayed in Fig. 4. For the lowest SAW power, the spatial PL distribution is almost identical to the case without a SAW. With increasing SAW power, additional PL emerges from $E$ and its intensity eventually exceeds the one at $G$ (at $x = 0$). The minimum modulation $\delta E_g^{min}$ required for transport can be extracted from the dependence of the PL intensity at $E$ on acoustic power [cf. Fig. 4(b)]. From the linear power density $P_\ell = 42$ W/m at the onset of transport (corresponding to $\delta E_g^{min} = 1$ meV cf. inset of Fig. 2), we estimate an exciton mobility $\mu_{ex} = v_{SAW}/(\delta E_g^{min} k_{SAW}) = 2.3 \times 10^4$ cm$^2$/(eV s). Through the Einstein relation, one obtains an exciton diffusion coefficient $D = \mu_{ex} k_B T = 24$ cm$^2$/s [9], which compares well with the predictions of Refs. [9,12] for a 16 nm-wide QW.

Further information about the spatial exciton distribution during transport can be extracted from the spectral shape of the PL along the transport path (cf. Fig. 5). The color plot in Fig. 5(a) displays the PL intensity as a function of position ($x$, vertical axis) and emission energy (horizontal axis) for a SAW excited with $P_{rf} = 24$ dBm.

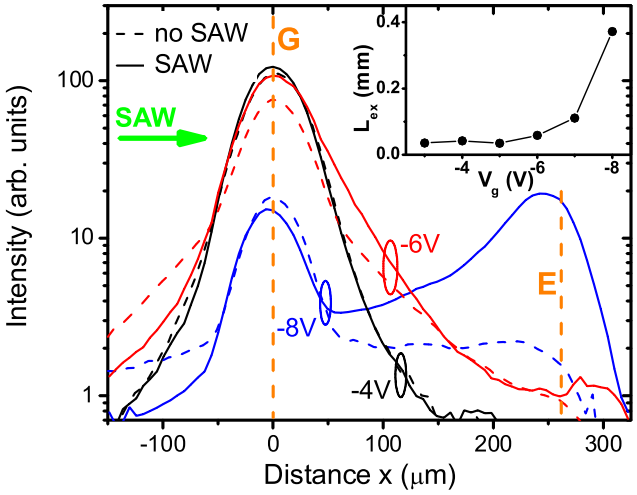


FIG. 3 (color online). Spatial PL profiles from indirect excitons for different gate voltages $V_g$ in the absence (dashed lines) and presence (solid lines) of a SAW with $P_{rf} = 24$ dBm. The inset shows the diffusion length $L_{ex}$ extracted from the decay of the profiles towards negative $x$. The positions $G$ and $E$ are defined in Fig. 1(b).

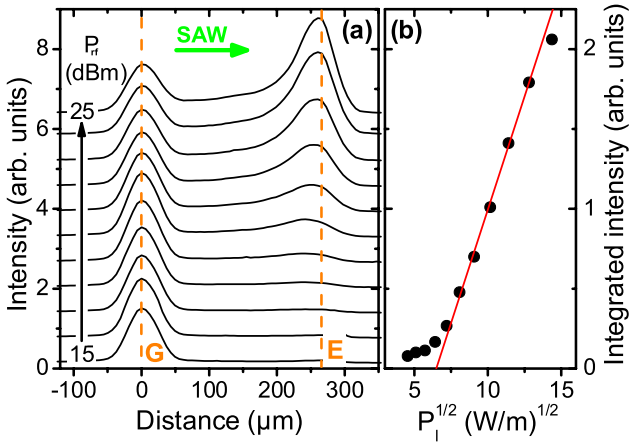


FIG. 4 (color online). (a) Spatially resolved PL profiles from indirect excitons for different applied rf power $P_{rf}$ and $V_g = -8$ V. (b) Integrated PL intensity at $E$ as a function of $\sqrt{P_\ell}$.

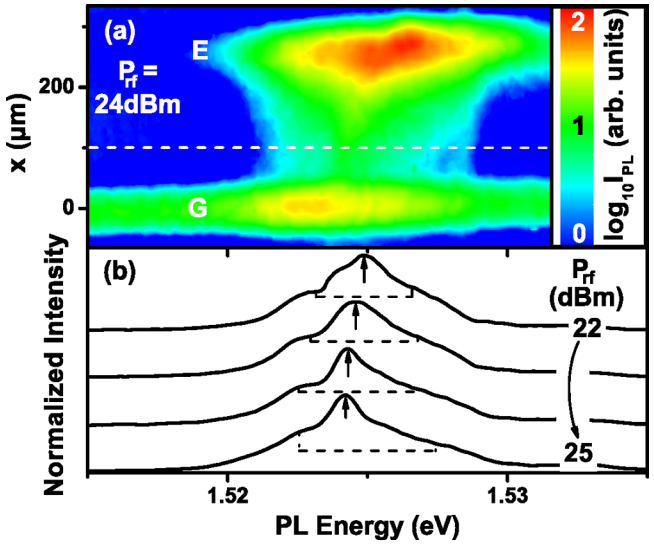


FIG. 5 (color online). (a) PL intensity as a function of transport distance $x$ (vertical scale) and energy (horizontal scale). (b) PL spectra recorded 100 $\mu$m away from $G$ for different $P_{rf}$ showing the emission from confined excitons (arrows). The dashed lines indicate the peak-to-peak band-gap modulation obtained from the inset of Fig. 2.

Figure 5(b) shows PL spectra recorded along the dashed line for different SAW powers. The emission cloud progressively blue shifts as one moves from the generation point ($G$, at $x = 0$) to the top-gate edge ($E$, at $x = 265$ $\mu$m). The blue shift is accounted for by the (i) screening of the applied bias $V_g$ by the high exciton density between $G$ and $E$ and the (ii) reduction of $V_g$ beyond $E$.

Photons arising from moving excitons acquire a finite in-plane wave vector $k_{ex} = v_{SAW} m^*_{ex}/\hbar$, where $m^*_{ex}$ is the effective exciton mass. Because of the finite $k_{ex}$, these photons suffer total reflection at the top surface and are not detected by our setup. The emission between $G$ and $E$ [cf. Figs. 3–5] is attributed to the recombination of excitons that have been captured by shallow traps in the DQW plane. The emission energy of trapped excitons reflects the momentary band gap $-\delta E_g \cos(\varphi_{SAW})$ [cf. Fig. 1(a)] at the emission time. The wide distribution of trapping times leads to the broad PL structure in Fig. 5(b) (dashed lines) extending from $E_{min}$ (corresponding to $\varphi_{SAW} = 0$) to $E_{max}$ ($\varphi_{SAW} = -\pi$). The sharp peaks marked by arrows, in contrast, are assigned to emission events taking place shortly after trapping. They reflect, therefore, the local concentration of moving excitons, which accumulate at the SAW phase $\varphi_{ex}$ where $v_{ex} = \mu_{ex} \nabla E_g(\varphi_{ex}) = v_{SAW}$ [i.e., for $\sin\varphi_{ex} = -v_{SAW}/(\mu_{ex} k_{SAW} \delta E_g)$]. The increased exciton density at $\varphi_{ex}$ (with $-\pi/2 < \varphi_{ex} < 0$) locally screens the applied bias, thus leading to enhanced PL emission at the energies indicated by the arrows. With increasing acoustic power, the sharp peaks redshift and sharpen as $|\varphi_{ex}|$ reduces and the moving excitons concentrate around this phase. A quantitative determination of the exciton distribution is hindered by the nontrivial dependence of $\tau_{ex}$ on density. From the width of the sharp peaks, however, we infer that most of the excitons are transported within a phase range $< \pi/3$, corresponding to a narrow stripe with a width $< \lambda_{SAW}/6 = 1$ $\mu$m parallel to the SAW wave fronts.

In conclusion, we have demonstrated the long-range transport of indirect excitons in GaAs DQWs by a SAW. The well-defined transport velocity together with the microscopic confinement and small exciton heating makes the SAW approach a promising tool for both fundamental research and possible applications of cold exciton gases.

We thank C. Hucho for helpful discussions as well as M. Höricke, B. Drescher, and W. Seidel for the growth and processing of the samples. Support from the nanoQUIT Consortium (BMBF, Germany) is gratefully acknowledged.

*rudolph@pdi-berlin.de

[1] J. M. Blatt, K. W. K. W. Böer, and W. Brandt, Phys. Rev. **126**, 1691 (1962).
[2] L. V. Keldysh and A. N. Kozlov, Sov. Phys. JETP **27**, 521 (1968).
[3] D. Snoke, Science **298**, 1368 (2002).
[4] L. V. Butov, J. Phys. Condens. Matter **16**, R1577 (2004).
[5] A. T. Hammack, M. Griswold, L. V. Butov, L. E. Smallwood, A. L. Ivanov, and A. C. Gossard, Phys. Rev. Lett. **96**, 227402 (2006).
[6] R. Rapaport, G. Chen, S. Simon, O. Mitrofanov, L. Pfeiffer, and P. M. Platzman, Phys. Rev. B **72**, 075428 (2005).
[7] Z. Vörös, R. Balili, D. W. Snoke, L. Pfeiffer, and K. West, Phys. Rev. Lett. **94**, 226401 (2005).
[8] P. C. M. Christianen, F. Piazza, J. G. S. Lok, J. C. Maan, and W. van der Vleuten, Physica (Amsterdam) **249–251B**, 624 (1998).
[9] A. Gärtner, A. W. Holleitner, J. P. Kotthaus, and D. Schuh, Appl. Phys. Lett. **89**, 052108 (2006).
[10] D. Sanvitto, F. Pulizzi, A. J. Shields, P. C. M. Christianen, S. N. Holmes, M. Y. Simmons, D. A. Ritchie, J. C. Maan, and M. Pepper, Science **294**, 837 (2001).
[11] D. W. Snoke, Y. Liu, Z. Vörös, L. Pfeiffer, and K. West, Solid State Commun. **134**, 37 (2005).
[12] Z. Vörös, D. W. Snoke, L. Pfeiffer, and K. West, Phys. Rev. Lett. **97**, 016803 (2006).
[13] C. Rocke, S. Zimmermann, A. Wixforth, J. P. Kotthaus, G. Böhm, and G. Weimann, Phys. Rev. Lett. **78**, 4099 (1997).
[14] M. Streibl, A. Wixforth, J. P. Kotthaus, A. O. Govorov, C. Kadow, and A. C. Gossard, Appl. Phys. Lett. **75**, 4139 (1999).
[15] T. Sogawa, P. V. Santos, S. K. Zhang, S. Eshlaghi, A. D. Wieck, and K. H. Ploog, Phys. Rev. B **63**, 121307(R) (2001).
[16] S. H. Simon, Phys. Rev. B **54**, 13 878 (1996).
[17] J. Rudolph, R. Hey, and P. V. Santos, Superlattices Microstruct. **41**, 293 (2007).